GEOLOGY

Million-year lag times in a post-orogenic sediment conveyor

R.-H. Fülöp[1,2]*, A. T. Codilean[1,3], K. M. Wilcken[2], T. J. Cohen[1,3], D. Fink[2], A. M. Smith[2], B. Yang[2], V. A. Levchenko[2], L. Wacker[4], S. K. Marx[1], N. Stromsoe[5], T. Fujioka[2†], T. J. Dunai[6]

Understanding how sediment transport and storage will delay, attenuate, and even erase the erosional signal of tectonic and climatic forcings has bearing on our ability to read and interpret the geologic record effectively. Here, we estimate sediment transit times in Australia's largest river system, the Murray-Darling basin, by measuring downstream changes in cosmogenic $^{26}Al/^{10}Be/^{14}C$ ratios in modern river sediment. Results show that the sediments have experienced multiple episodes of burial and reexposure, with cumulative lag times exceeding 1 Ma in the downstream reaches of the Murray and Darling rivers. Combined with low sediment supply rates and old sediment blanketing the landscape, we posit that sediment recycling in the Murray-Darling is an important and ongoing process that will substantially delay and alter signals of external environmental forcing transmitted from the sediment's hinterland.

INTRODUCTION

Earth's dynamic surface is the product of tectonic processes and climate (*1*–*3*). Tectonic forces create mountains, while erosion breaks the rocks down to sediment that is evacuated by rivers and eventually ends up in the world's oceans. Rivers are the world's large sediment conveyor belts, and recent estimates suggest that more than 20 billion tonnes of particulate sediments are delivered to the global ocean every year (*4*). A similar amount of dissolved sediment is also transported, controlling the ocean's bulk geochemical composition and so determining the amount of nutrients and biological productivity (*5*, *6*). Rivers also transmit signals of external environmental forcing: Each parcel of sediment carries information about the geology, geomorphology, and the climate of the contributing upland areas (*7*, *8*). These "environmental signals" result in changes in the sediment flux and are carried by mineralogical, textural, or geochemical proxies that record the response of the landscape to external forcings. Environmental signals may be altered and, in some instances, even destroyed—or "shredded"—by the internal dynamics of the sediment routing system (*9*, *10*). Quantifying the dynamics of sediment routing systems is essential to understanding the mass fluxes associated with the physical, biological, and chemical processes acting across the landscape (*11*, *12*), just as it is central to how we read and interpret the global record of Earth history (*13*). Deciphering the latter, in turn, requires an understanding of how the erosional response of landscapes to climatic and tectonic forcings is buffered, modified, and even erased entirely by the world's large rivers as the sediments are transferred from source areas to depocenters.

Burial dating is a means of dating geological deposits by the analysis of a pair of cosmogenic radionuclides—rare isotopes produced by cosmic ray bombardment of surface rocks (*14*). Upon burial and cessation of nuclide production, the differential decay of the two nuclides results in a change in their initial ratio in proportion to the duration of burial. In modern river sediment, burial ages are "apparent" ages and represent a measure of the time that the sediment has spent in storage. The most common nuclide pair used in burial dating is ^{26}Al and ^{10}Be, with a production ratio in quartz of Al/Be = ~7 (*15*), and a useful age range of 0.5 to 6 Ma (*16*). The latter is dictated by the nuclides' half-lives of 0.7 and 1.39 Ma, respectively. By adding a third nuclide—in situ ^{14}C—with a substantially shorter half-life (5730 years), the minimum resolvable sediment residence time can be reduced to the order of 10^3 to 10^4 years. Cosmogenic $^{26}Al/^{10}Be$ ratios in sediment from large river basins have been used to elucidate the fate of sediment transported from source to sink. For example, samples from the lower reaches of the Amazon yield $^{26}Al/^{10}Be$ ratios of 3.8 to 5.5 (*17*), interpreted as the mixing of fresh sediment sourced from the Andes with sediment of Miocene age stored in floodplains. It is argued that because the sediment flux of the Amazon is dominated by Andean sources (*18*) and despite the mixing of fresh and old sediment, cosmogenic ^{10}Be signals reaching the Atlantic are representative of the Andean hinterland (*17*). The same has been shown for other orogenic settings, such as the Ganga (*19*) and the Po (*20*). The inference being downstream sediment can be used to elucidate upstream environmental conditions, sediment production in these examples. However, not every sediment routing system starts with a 6-km orogen at its source. Post-orogenic landscapes that occupy a large proportion of the Earth's surface and contribute roughly half of the global sediment flux (*21*) will have, on average, lower relief, dryer climate, and lower rates of geomorphic activity. It is here that the potential for substantial buffering of the erosional response of landscapes to external environmental forcings is the highest.

RESULTS

We measured in situ produced cosmogenic ^{26}Al, ^{10}Be, and ^{14}C in modern sediment from the Murray-Darling basin (MDB), to quantify downstream changes in sediment residence times along the river system. Australia's tectonically passive post-Cretaceous history means

[1]School of Earth, Atmospheric and Life Sciences, University of Wollongong, Wollongong, NSW 2522, Australia. [2]Australia's Nuclear Science and Technology Organisation (ANSTO), Lucas Heights, NSW 2234, Australia. [3]ARC Centre of Excellence for Australian Biodiversity and Heritage, University of Wollongong, Wollongong, NSW 2522, Australia. [4]Ion Beam Physics, ETH-Zürich, Zürich 8093, Switzerland. [5]College of Engineering, IT and Environment, Charles Darwin University, Darwin, NT 0909, Australia. [6]Institute of Geology and Mineralogy, University of Cologne, Cologne 50674, Germany.
*Corresponding author. Email: rfulop@uow.edu.au
†Present address: Centro Nacional de Investigación sobre la Evolución Humana (CENIEH), Burgos 09002, Spain.

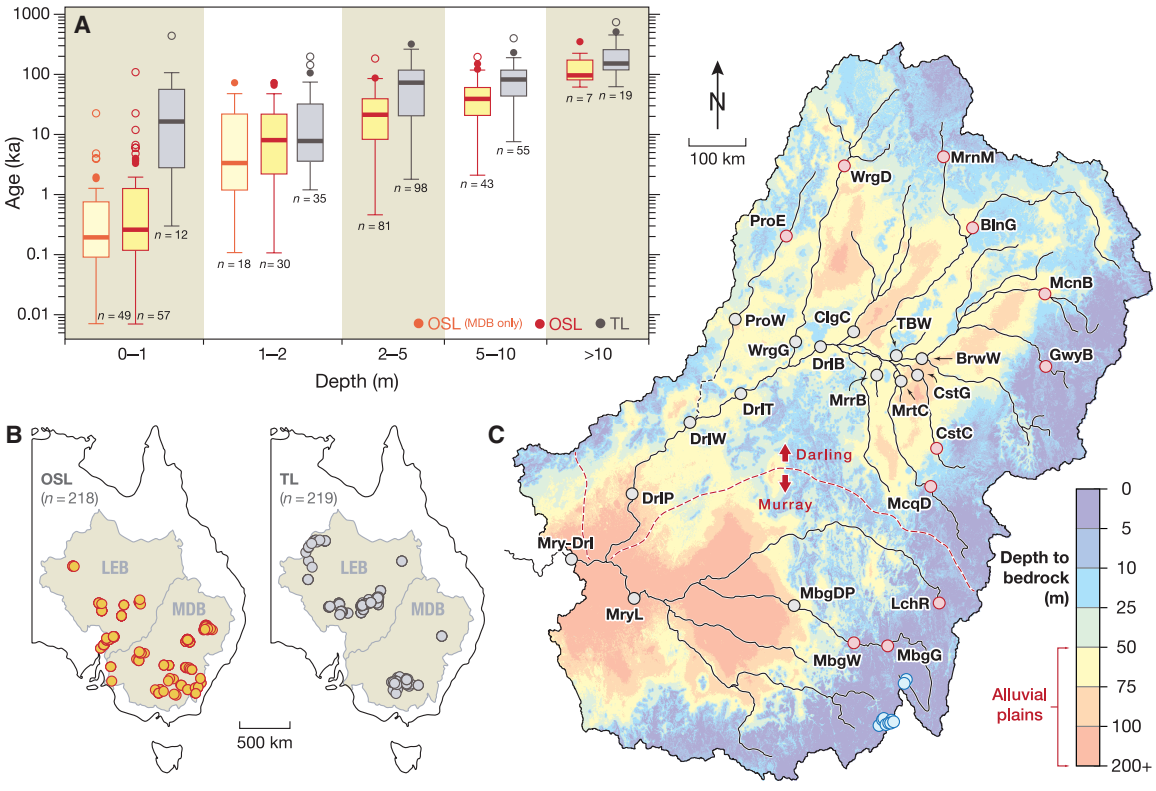

Fig. 1. Compilation of luminescence ages, a regolith depth map of the MDB, and location of sample sites. (**A** and **B**) Optically stimulated luminescence (OSL) and thermoluminescence (TL) ages in MDB and the LEB fluvial deposits taken from the OCTOPUS database (*22*) and maps showing their spatial distribution. (**C**) Map of the MDB showing the distribution of regolith depth (*24*) and the location of sample sites for cosmogenic radionuclide analyses. Blue circles are headwater samples, red circles are upland samples, and black circles are lowland samples. The red dashed line shows the approximate boundary between the Murray (south) and Darling (north) sub-basins. On the regolith depth map, the colors yellow, orange, and red demarcate the approximate extent of the alluvial plains (*24*, *25*).

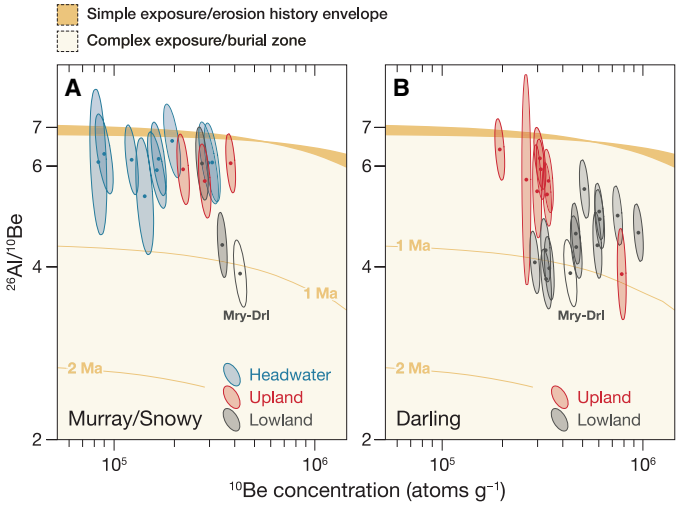

Fig. 2. Cosmogenic ^{26}Al/^{10}Be burial plots. (**A**) Murray Basin samples (including the Snowy River). (**B**) Darling Basin samples. Samples that have experienced continuous exposure to cosmic radiation will plot within the orange envelope. Samples that have experienced a complex exposure history involving one or more episodes of burial and cessation of nuclide production (i.e., samples undergoing storage) will plot in the yellow shaded area. The distance between the simple exposure/erosion history envelope and a data point is proportional to the duration of burial, with samples buried for longer plotting further away from the orange envelope. Orange curves show 1- and 2-Ma burial isochrons. Uncertainties (ellipses) are shown at the 2σ level. Colors indicate sample provenance, as shown in Fig. 1.

that it has the lowest relief and mean elevation of all the continents. Its two largest inland drainage basins—the MDB and the Lake Eyre basin (LEB) (Fig. 1)—function as vast sediment-conveyors of mass flux from source to sink, draining ~30% of the continent's landmass. Both MDB and LEB rivers traverse extensive alluvial plains blanketed by a thick layer of unconsolidated sediment (Fig. 1). Luminescence dating of over 430 fluvial samples (*22*) shows that these sediments have deposition ages of anywhere between 10^2 to 10^4 years for deposits close to the surface and older than 10^5 years for deposits at depths of >10 m (Fig. 1). The ubiquity of "old" sediment blanketing the landscape combined with the low relief and low sediment fluxes that characterize arid Australia's rivers (*23*) implies that reworking of floodplain material could substantially alter signals of environmental forcings—such as, for example, the erosional response to Quaternary paleoclimate variability—traveling from source to sink.

We collected and analyzed a total of 36 modern river sediment samples: 10 from the headwaters of the Murray, Murrumbidgee, and Snowy rivers, draining the Snowy Mountains with the highest elevations on the continent; 5 from the Murray River sub-basin; 20 from the Darling River sub-basin; and 1 sample downstream of the confluence of the Murray and Darling rivers. Our aim was to sample rivers both upstream (Fig. 1C, red circles)—referred to here as "upland samples"—and downstream (Fig. 1C, black circles)—referred to here as "lowland samples"—of the vast alluvial plains that characterize this landscape. We delineate the approximative extent of the alluvial plains using a regolith depth map (Fig. 1) produced

from a continent-wide database of >128,000 drillhole records (*24*). The extent of the alluvial plains also coincides with those of Australia's Cenozoic sedimentary basins that have been extensively mapped (*25*). The MDB occupies an area of 1 million km^2, and the location of sample sites was ultimately influenced by distance, access to the channel, and the presence of anthropogenic features, such as dams. Overall, however, our sample set provides comprehensive coverage of the MDB. We measured ^{10}Be in all samples and ^{26}Al in all but one of the headwater samples (BGC). Because of the time consuming and experimental nature of in situ ^{14}C analyses, we only measured ^{14}C in a subset of 14 samples that were representative of both upland and lowland samples from both the Darling and Murray sub-basins.

Obtained ^{26}Al/^{10}Be ratios in the samples range between 3.8 and 6.5 (Fig. 2 and table S1). All but one sample plot in the complex exposure/burial zone in Fig. 2 (yellow shaded area), indicating burial. However, because of large uncertainties, apparent burial ages cannot be resolved for the headwater samples collected from the Murray and Snowy basins (Fig. 2A, blue). Overall, samples collected from the lowland reaches of the Murray and Darling show lower ^{26}Al/^{10}Be ratios than those from the upland reaches, consistent with an increase in the likelihood of storage and reworking of floodplain material as sediment moves downstream traversing the extensive alluvial plains. The largest apparent burial age is obtained for the lowermost sample collected from the Darling River, namely, DrlP at ~1.2 ± 0.3 (2σ) Ma (table S1). Seven other samples produce apparent burial ages on the order of 1 Ma, including ProE collected from the upstream reaches of the Paroo River (table S1). Apparent burial ages were calculated using a simple model that assumes one single burial event and complete shielding from cosmic radiation during burial. Given that it is unlikely for burial during sediment transport to be deep enough to shield sediment from cosmic radiation completely, these apparent burial ages should be interpreted as minimum sediment storage durations [c.f. (*17*)]. On average, ^{10}Be abundances are higher in the Darling sub-basin samples by comparison to the Murray. This indicates lower sediment production rates in the Darling, which is again consistent with the larger apparent burial ages obtained for this basin, as the less fresh sediment is carried by rivers, the more ^{26}Al/^{10}Be ratios will be affected by reworking of old floodplain material.

Because of its short half-life, no in situ produced ^{14}C should be present in any sample that has experienced an episode of complete burial for longer than a few tens of thousand years. Further, fluvial

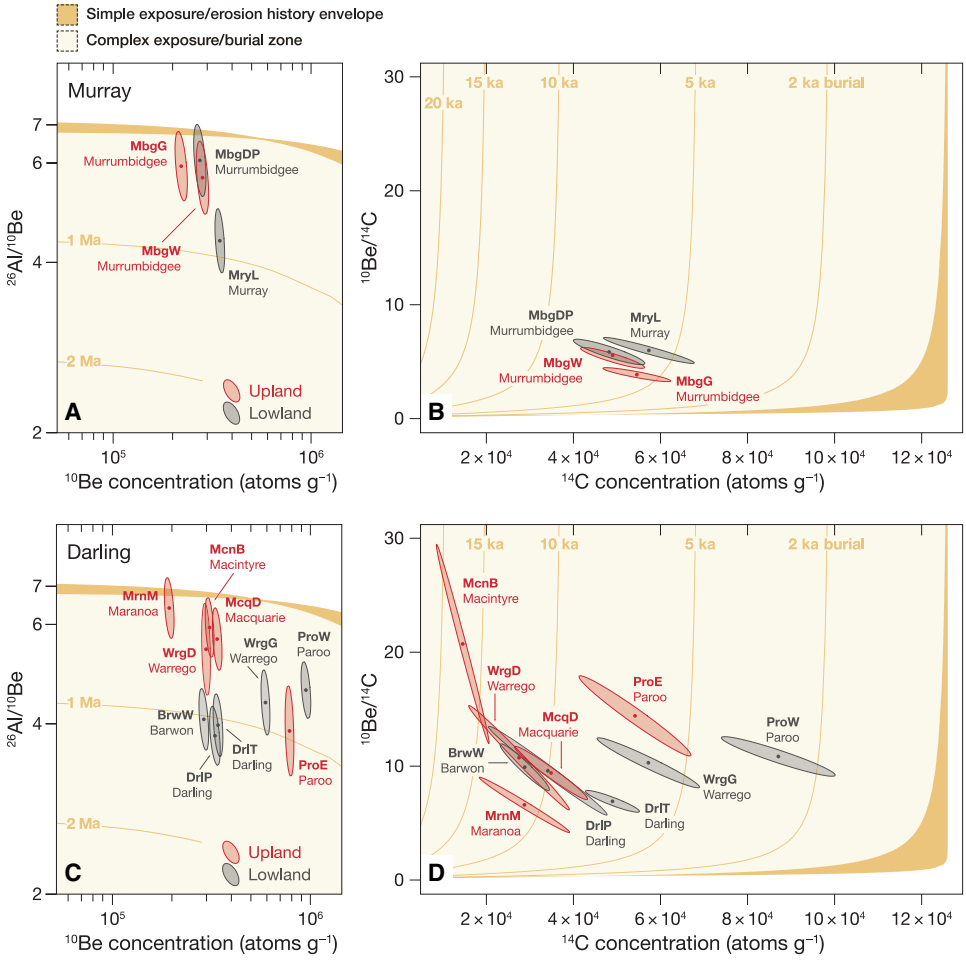

Fig. 3. Cosmogenic ^{26}Al/^{10}Be/^{14}C burial plots. (**A** and **B**) Murray Basin samples. (**C** and **D**) Darling Basin samples. (A) and (C) are the same as Fig. 2 but only show those samples where ^{26}Al, ^{10}Be, and ^{14}C were analyzed to allow for easy comparison between ^{26}Al/^{10}Be and ^{10}Be/^{14}C ratios. Samples that have experienced a complex exposure history (i.e., samples undergoing storage) will plot in the yellow shaded area. Uncertainties are shown at 2σ level, and orange curves show burial isochrons. Colors indicate sample provenance, as shown in Fig. 1.

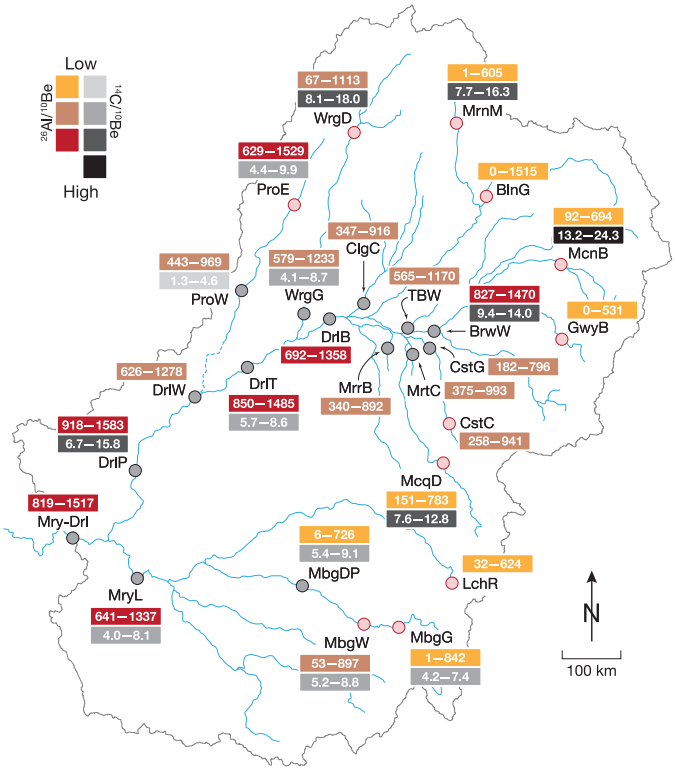

Fig. 4. Drainage network and distribution of apparent burial ages. Orange and red shaded boxes show ^{26}Al/^{10}Be age ranges, and black and gray shaded boxes show ^{14}C/^{10}Be age ranges. Ages are expressed in thousand years, and age ranges represent 95% confidence intervals. Red circles are upland samples, and black circles are lowland samples.

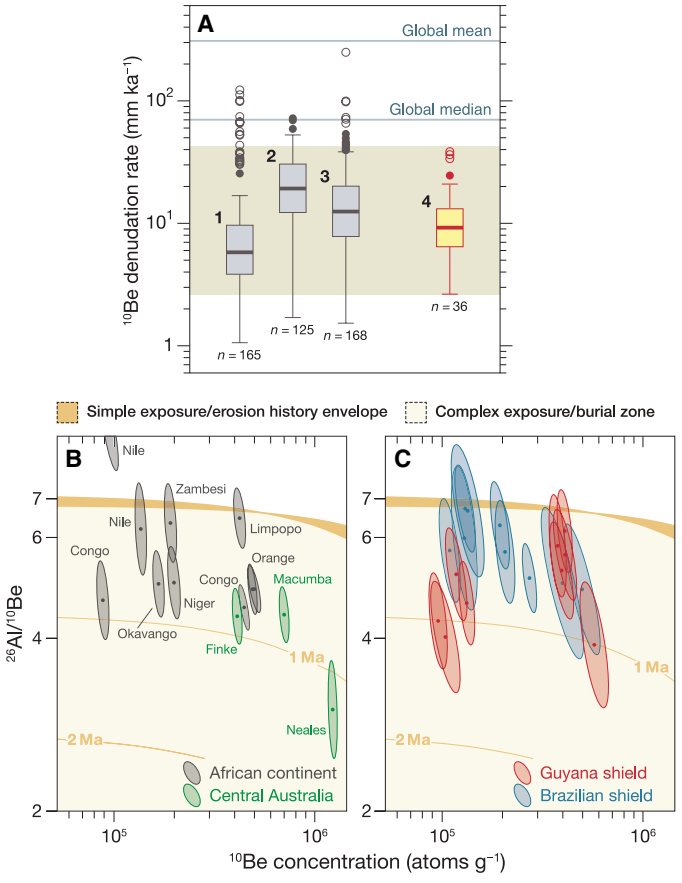

Fig. 5. ^{10}Be-based denudation rates and ^{26}Al/^{10}Be ratios recorded in rivers draining Australia and other Gondwana segments. (**A**) Comparison of published ^{10}Be-based denudation rates (*22*) with those recorded in the MDB (this study): 1, Africa; 2, the Western Ghat Mountains of India; 3, the Brazilian Atlantic continental margin and the Guyana and Brazilian shields; 4, MDB. Horizontal lines show the global median and mean denudation rates calculated using the OCTOPUS database (*22*). Horizontal band indicates the range of MDB denudation rates. (**B** and **C**) Cosmogenic ^{26}Al/^{10}Be burial plots showing published ^{26}Al and ^{10}Be data for (B) large rivers draining the African continent and central Australia (*33*) and (C) rivers draining the Guyana and Brazilian shields (*17*). Note how virtually all samples in (B) and (C) plot in the yellow shaded area indicating a complex exposure history. Uncertainties are shown at 2σ level, and orange curves show burial isochrons.

sediment samples that were buried for long enough to lose all their initial ^{14}C, and then are reexposed to cosmic radiation, should show ^{10}Be/^{14}C ratios that are consistent with a simple exposure-erosion scenario, i.e., ratios plotting within the orange envelope in Fig. 3. Contrary to the above, none of the samples that we analyzed, including those with apparent ^{26}Al/^{10}Be burial ages of ~1 Ma, were depleted in ^{14}C. Moreover, all samples produced ^{10}Be/^{14}C ratios that plot inside the complex exposure/burial zone, indicating burial (Fig. 3 and table S2). Obtained apparent ^{10}Be/^{14}C burial ages range between 2.7 (−1.5/+1.6; 2σ) ka and 20.0 (−4.3/+8.5; 2σ) ka and, as with the ^{26}Al/^{10}Be ages, should be interpreted as minimum sediment storage durations. Together, the ^{26}Al/^{10}Be/^{14}C data imply that the sediment must have experienced multiple episodes of burial and reexposure to cosmic radiation.

DISCUSSION

Sediment pathways from source to sink are complex, and this complexity is saliently illustrated by our results. Albeit not fully resolvable using the ^{26}Al/^{10}Be pair, all headwater samples indicate a burial signal, suggesting that following detachment from bedrock, sediment may experience lengthy storage in regolith mantles, finding that corroborates previous studies (*26*, *27*). While there is uniformity in both ^{10}Be abundances and ^{26}Al/^{10}Be ratios among upland samples from both Murray and Darling and these are also similar to the ^{26}Al/^{10}Be ratios of the headwater samples, lowland samples show more variability in both isotopic abundances and ratios. This variability in lowland sample ^{26}Al/^{10}Be ratios and concentrations is what one would expect in a system where sediment storage is important and mainly reflects the extent of the alluvial plains traversed by the various rivers (Fig. 1C) and, to a lesser extent but still important, the drainage pattern. For example, ^{26}Al/^{10}Be ratios range between 6.2 and 4.1 for samples collected from tributaries of the Darling upstream of sample DrlB; however, between DrlB and DrlP, a stretch of ~500 km where the alluvial plain is more constrained and the Darling has few tributaries except the Warrego and Paroo Rivers, ^{26}Al/^{10}Be ratios have a narrower range (3.8 to 4.3) and are virtually identical within analytical uncertainty. Moreover, there is a lack of covariance between ^{26}Al/^{10}Be and ^{10}Be/^{14}C ratios (Figs. 2 and 3), especially in the Darling sub-basin samples. In those samples, ^{26}Al/^{10}Be ratios indicate an increase in apparent burial ages between upland and lowland samples (Fig. 4), whereas ^{10}Be/^{14}C ratios show the opposite, namely, lowland samples have lower ^{10}Be/^{14}C apparent burial ages than upland samples, in addition to showing considerable

variability (Fig. 4). The discordance between $^{26}Al/^{10}Be$ and $^{10}Be/^{14}C$ ratios, combined with the antiquity of the sediment blanketing the landscape (Fig. 1A), suggests that reworking of old sediment in the MDB is an important and ongoing process that will substantially modify the erosional record of environmental forcings transmitted from the sediment's hinterland.

Millennial lag times in sediment routing systems are not uncommon, and sediment buffering has now been documented to occur prolifically even in the mountain source regions of Himalayan rivers (*28*–*31*). Here, glacially scoured and overdeepened intermontane basins provide ample accommodation space for sediment storage in floodplains, fans, and terraces. Notwithstanding the large valley fills, buffering in orogenic settings likely occurs over 10^3- to 10^4-year time scales (*28*, *31*), and combined with the high sediment production rates and sediment fluxes characteristic for orogenic settings (*22*) means that signals of environmental forcings—such as the ^{10}Be record of mountain erosion—may be effectively transmitted from source to sink (*32*, *33*). In contrast to tectonically active mountain belts, post-orogenic landscapes will have low sediment production rates and therefore also reduced sediment fluxes (Fig. 5). The low topographic relief of these landscapes also means that the amplitude of environmental signals will be subdued and rivers will have a reduced capacity to transport sediment. The latter facilitates long sediment transit times, while the former means that recycling of old sediment will readily alter erosional signals of environmental forcing transmitted from the sediment's hinterland. The 10^3- to 10^4-year lag times documented in orogenic settings are short compared to the ~1-Ma lag times recorded in this study. Further, similarly long lag times can be inferred from $^{26}Al/^{10}Be$ ratios recorded in other large rivers draining the post-orogenic landscapes that characterize Australia and other Gondwana segments (Fig. 5). On the basis of these $^{26}Al/^{10}Be$ ratios and similarities in sediment production rates across these post-orogenic landscapes (Fig. 5), we posit that the million-year lag times and the alteration of erosional signals of environmental forcings traveling from source to sink by reworking of old sediment is a characteristic feature of post-orogenic sediment routing systems, globally. The above, in turn, may limit the amount of interpretation possible from sediments deposited on the continental margins of tectonically quiescent continents such as Africa and Australia.

MATERIALS AND METHODS

Cosmogenic ^{26}Al and ^{10}Be analyses

Sediment was sieved in the field to isolate the 250- to 500-μm fraction for analysis, and quartz was isolated using froth flotation to separate feldspars from quartz and dilute HF/HNO_3 acid mixture to remove meteoric ^{10}Be and further purify the quartz. Be and Al were separated at the University of Wollongong following procedures described in von Blanckenburg *et al.* (*34*) with the modification that Al was separated from Be and Ti using pH-sensitive precipitation before Be cation exchange chromatography. Samples were spiked with ~300 μg of ^9Be from a low-level beryl carrier solution added before complete HF dissolution.

$^{10}Be/^9Be$ and $^{26}Al/^{27}Al$ ratios were measured using the 10MV ANTARES and 6MV SIRIUS accelerator mass spectrometer (AMS) facilities at Australia's Nuclear Science and Technology Organisation (ANSTO). The native Al concentrations of the samples ranged from 70 to 370 parts per million (ppm) (median, 138 ppm) and were determined via inductively coupled plasma optical emission spectrometry (ICP-OES) with a precision of 3 to 4%. Analytical uncertainties for the final ^{10}Be and ^{26}Al concentrations (atoms g^{-1}) include AMS measurement uncertainties (larger of counting statistics or SD of repeats and blank corrections) in quadrature with 1 to 2% for ^{10}Be and 2 to 3% for ^{26}Al standard reproducibility (depending on the individual AMS measurement conditions), 1% uncertainty in the ^9Be carrier concentration, and 4% uncertainty in the ICP-OES Al measurements. Results of the ^{26}Al and ^{10}Be analyses, including measurement uncertainties and blank corrections, are summarized in table S1.

In situ cosmogenic ^{14}C analyses

^{14}C was extracted from quartz at the ANSTO–University of Wollongong in situ ^{14}C extraction laboratory (*35*), housed at ANSTO. The ^{14}C extraction scheme exploits the high temperature phase transformation of quartz to cristobalite to quantitatively extract the carbon as CO_2 (*36*). The extraction procedure consists of (i) leaching the ultrapure quartz aliquot using HNO_3; (ii) in vacuo heating at 600°C for 2 hours in fused silica tubes to remove meteoric ^{14}C; tubes are subsequently sealed (addition of a solid carbonate carrier may be required at this step when insufficient CO_2 would be released from a sample); (iii) heating at 1650°C for 2 hours in the sealed fused silica tubes under a continuous flow of nitrogen gas, to transform the quartz to cristobalite and release ^{14}C as CO_2; (iv) in vacuo cracking of the tubes; cleaning of the released gas and quantifying the mass of CO_2.

Following extraction and cleaning, the CO_2 gas is converted to graphite using ANSTO's in-house built laser-heated microfurnace. This setup allows for the graphitization of microgram-sized carbon samples containing between 5 and 60 μg of carbon, with conversion efficiencies for 5-μg targets ranging from 80 to 100% (*37*). Graphite targets were analyzed using ANSTO's 10MV ANTARES tandem accelerator. To test for the effects of the graphitization process, splits from the extracted and cleaned CO_2 gas from blanks, laboratory intercomparison materials, and some of the samples were also measured using the gas ion source of the MICADAS AMS facility at ETH-Zürich. The MICADAS setup allows for the analysis of CO_2 samples between 3 and 100 μg of carbon, sealed in glass tubes (*38*).

Results of the in situ ^{14}C analyses, including measurement uncertainties and blank corrections, are summarized in table S2. Measurements of system blanks and reproducibly using CRONUS intercomparison materials that were run with the samples are presented in Fülöp *et al.* (*35*). The reproducibility of sample ^{14}C results was also tested by measuring duplicates for seven of the samples and triplicates for a further three (fig. S1). Where duplicate or triplicate measurements were performed, Fig. 3 plots $^{10}Be/^{14}C$ ratios calculated using average ^{14}C concentrations.

Apparent denudation rate and apparent burial age calculations

Denudation rates were calculated with the open-source program CAIRN v.1 (*39*) using default settings for all parameters and a hydrologically enforced 250-m digital elevation model of the MDB. Calculated denudation rates are apparent rates and do not account for any decay of ^{10}Be or ^{26}Al. These rates are not used in this study as such and are provided here for comparison with other regions. Apparent burial ages were calculated with CosmoCalc v.3.0 (*40*) using parameters that matched those used with CAIRN, namely, Lal/Stone scaling factors and Braucher neutron and muon production approximations. We also use CosmoCalc to calculate burial-corrected denudation rates (tables S1 and S2). Burial ages are apparent

ages as they are calculated following a simple single exposure–complete burial model and should be interpreted as minimum sediment storage durations.

SUPPLEMENTARY MATERIALS

Supplementary material for this article is available at http://advances.sciencemag.org/cgi/content/full/6/25/eaaz8845/DC1

REFERENCES AND NOTES

1. P. Molnar, P. England, Late Cenozoic uplift of mountain ranges and global climate change: Chicken or egg. *Nature* **346**, 29–34 (1990).
2. M. E. Raymo, W. F. Ruddiman, Tectonic forcing of late Cenozoic climate. *Nature* **359**, 117–122 (1992).
3. K. X. Whipple, The influence of climate on the tectonic evolution of mountain belts. *Nat. Geosci.* **2**, 97–104 (2009).
4. J. D. Milliman, K. L. Farnsworth, *River Discharge to the Coastal Ocean: A Global Synthesis* (Cambridge Univ. Press, 2011).
5. N. Kumar, R. F. Anderson, R. A. Mortlock, P. N. Froelich, P. Kubik, B. Dittrich-Hannen, M. Suter, Increased biological productivity and export production in the glacial Southern Ocean. *Nature* **378**, 675–680 (1995).
6. T. D. Jickells, Z. S. An, K. K. Andersen, A. R. Baker, G. Bergametti, N. Brooks, J. J. Cao, P. W. Boyd, R. A. Duce, K. A. Hunter, H. Kawahata, N. Kubilay, J. laRoche, P. S. Liss, N. Mahowald, J. M. Prospero, A. J. Ridgwell, I. Tegen, R. Torres, Global iron connections between desert dust, ocean biogeochemistry, and climate. *Science* **308**, 67–71 (2005).
7. P. A. Allen, From landscapes into geological history. *Nature* **451**, 274–276 (2008).
8. B. W. Romans, S. Castelltort, J. A. Covault, A. Fildani, J. Walsh, Environmental signal propagation in sedimentary systems across timescales. *Earth Sci. Rev.* **153**, 7–29 (2016).
9. D. J. Jerolmack, C. Paola, Shredding of environmental signals by sediment transport. *Geophys. Res. Lett.* **37**, L19401 (2010).
10. J. J. Armitage, R. A. Duller, A. C. Whittaker, P. A. Allen, Transformation of tectonic and climatic signals from source to sedimentary archive. *Nat. Geosci.* **4**, 231–235 (2011).
11. G. L. Foster, D. Vance, Negligible glacial–interglacial variation in continental chemical weathering rates. *Nature* **444**, 918–921 (2006).
12. D. Vance, D. A. H. Teagle, G. L. Foster, Variable quaternary chemical weathering fluxes and imbalances in marine geochemical budgets. *Nature* **458**, 493–496 (2009).
13. P. Zhang, P. Molnar, W. R. Downs, Increased sedimentation rates and grain sizes 2–4 Myr ago due to the influence of climate change on erosion rates. *Nature* **410**, 891–897 (2001).
14. D. E. Granger, P. Muzikar, Dating sediment burial with in situ-produced cosmogenic nuclides: Theory, techniques, and limitations. *Earth Planet. Sci. Lett.* **188**, 269–281 (2001).
15. L. B. Corbett, P. R. Bierman, D. H. Rood, M. W. Caffee, N. A. Lifton, T. E. Woodruff, Cosmogenic ^{26}Al/^{10}Be surface production ratio in Greenland. *Geophys. Res. Lett.* **44**, 1350–1359 (2017).
16. D. E. Granger, M. Schaller, Cosmogenic nuclides and erosion at the watershed scale. *Elements* **10**, 369–373 (2014).
17. H. Wittmann, F. von Blanckenburg, L. Maurice, J. L. Guyot, P. W. Kubik, Recycling of Amazon floodplain sediment quantified by cosmogenic ^{26}Al and ^{10}Be. *Geology* **39**, 467–470 (2011).
18. R. H. Meade, T. Dunne, J. E. Richey, U. M. Santos, E. Salati, Storage and remobilization of suspended sediment in the lower Amazon River of Brazil. *Science* **228**, 488–490 (1985).
19. M. Lupker, P.-H. Blard, J. Lavé, C. France-Lanord, L. Leanni, N. Puchol, J. Charreau, D. Bourlès, ^{10}Be-derived Himalayan denudation rates and sediment budgets in the Ganga basin. *Earth Planet. Sci. Lett.* **333–334**, 146–156 (2012).
20. H. Wittmann, M. G. Malusà, A. Resentini, E. Garzanti, S. Niedermann, The cosmogenic record of mountain erosion transmitted across a foreland basin: Source-to-sink analysis of in situ ^{10}Be, ^{26}Al and ^{21}Ne in sediment of the Po river catchment. *Earth Planet. Sci. Lett.* **452**, 258–271 (2016).
21. J. K. Willenbring, A. T. Codilean, B. J. McElroy, Earth is (mostly) flat: Apportionment of the flux of continental sediment over millennial time scales. *Geology* **41**, 343–346 (2013).
22. A. T. Codilean, H. Munack, T. J. Cohen, W. M. Saktura, A. Gray, S. M. Mudd, OCTOPUS: An open cosmogenic isotope and luminescence database. *Earth Syst. Sci. Data* **10**, 2123–2139 (2018).
23. A. Habeck-Fardy, G. C. Nanson, Environmental character and history of the Lake Eyre basin, one seventh of the Australian continent. *Earth Sci. Rev.* **132**, 39–66 (2014).
24. J. R. Wilford, R. Searle, M. Thomas, D. Pagendam, M. J. Grundy, A regolith depth map of the Australian continent. *Geoderma* **266**, 1–13 (2016).
25. R. P. Langford, G. E. Wilford, E. M. Truswell, A. R. Isern, *Palaeogeographic Atlas of Australia, Volume 10 – Cainozoic* (Australian Geological Survey Organisation, 1995).
26. M. Struck, J. D. Jansen, T. Fujioka, A. T. Codilean, D. Fink, D. L. Egholm, R.-H. Fülöp, K. M. Wilcken, S. Kotevski, Soil production and transport on postorogenic desert hillslopes quantified with ^{10}Be and ^{26}Al. *Geol. Soc. Am. Bull.* **130**, 1017–1040 (2018).
27. P. O. Suresh, A. Dosseto, P. P. Hesse, H. K. Handley, Very long hillslope transport timescales determined from uranium-series isotopes in river sediments from a large, tectonically stable catchment. *Geochim. Cosmochim. Acta* **142**, 442–457 (2014).
28. J. H. Blöthe, O. Korup, Millennial lag times in the Himalayan sediment routing system. *Earth Planet. Sci. Lett.* **382**, 38–46 (2013).
29. P. D. Clift, L. Giosan, Sediment fluxes and buffering in the post–glacial Indus Basin. *Basin Res.* **26**, 369–386 (2014).
30. H. Munack, J. H. Blöthe, R. H. Fülöp, A. T. Codilean, D. Fink, O. Korup, Recycling of Pleistocene valley fills dominates 135 ka of sediment flux, upper Indus River. *Quat. Sci. Rev.* **149**, 122–134 (2016).
31. T. N. Jonell, L. A. Owen, A. Carter, J.-L. Schwenniger, P. D. Clift, Quantifying episodic erosion and transient storage on the western margin of the Tibetan Plateau, upper Indus River. *Quatern. Res.* **89**, 281–306 (2018).
32. H. Wittmann, F. von Blanckenburg, The geological significance of cosmogenic nuclides in large lowland river basins. *Earth Sci. Rev.* **159**, 118–141 (2016).
33. H. Wittmann, M. Oelze, J. Gaillardet, E. Garzanti, F. von Blanckenburg, A global rate of denudation from cosmogenic nuclides in the Earth's largest rivers. *Earth Sci. Rev.* **204**, 103147 (2020).
34. F. von Blanckenburg, N. S. Belshaw, R. K. O'Nions, Separation of ^{9}Be and cosmogenic ^{10}Be from environmental materials and SIMS isotope dilution analysis. *Chem. Geol.* **129**, 93–99 (1996).
35. R.-H. Fülöp, D. Fink, B. Yang, A. T. Codilean, A. M. Smith, L. Wacker, V. A. Levchenko, T. J. Dunai, The ANSTO – University of Wollongong in-situ ^{14}C extraction laboratory. *Nucl. Instrum. Methods Phys. Res. Sect. B* **438**, 207–213 (2019).
36. R.-H. Fülöp, L. Wacker, T. J. Dunai, Progress report on a novel in situ ^{14}C extraction scheme at the University of Cologne. *Nucl. Instrum. Methods Phys. Res. Sect. B* **361**, 20–24 (2015).
37. B. Yang, A. M. Smith, S. Long, Second generation laser-heated microfurnace for the preparation of microgram-sized graphite samples. *Nucl. Instrum. Methods Phys. Res. Sect. B* **361**, 363–371 (2015).
38. L. Wacker, S. M. Fahrni, I. Hajdas, M. Molnar, H.-A. Synal, S. Szidat, Y. L. Zhang, A versatile gas interface for routine radiocarbon analysis with a gas ion source. *Nucl. Instrum. Methods Phys. Res. Sect. B* **294**, 315–319 (2013).
39. S. M. Mudd, M.-A. Harel, M. D. Hurst, S. W. D. Grieve, S. M. Marrero, The CAIRN method: Automated, reproducible calculation of catchment-averaged denudation rates from cosmogenic nuclide concentrations. *Earth Surf. Dyn.* **4**, 655–674 (2016).
40. P. Vermeesch, CosmoCalc: An Excel add-in for cosmogenic nuclide calculations. *Geochem. Geophys. Geosyst.* **8**, Q08003 (2007).
41. D. Fink, A. Smith, An inter-comparison of ^{10}Be and ^{26}Al AMS reference standards and the ^{10}Be half-life. *Nucl. Instrum. Methods Phys. Res. Sect. B* **259**, 600–609 (2007).
42. K. M. Wilcken, T. Fujioka, D. Fink, R.-H. Fülöp, A. T. Codilean, K. Simon, C. Mifsud, S. Kotevski, SIRIUS Performance: ^{10}Be, ^{26}Al and ^{36}Cl measurements at ANSTO. *Nucl. Instrum. Methods Phys. Res. Sect. B* **455**, 300–304 (2019).
43. K. Nishiizumi, M. Imamura, M. W. Caffee, J. R. Southon, R. C. Finkel, J. McAninch, Absolute calibration of ^{10}Be AMS standards. *Nucl. Instrum. Methods Phys. Res. Sect. B* **258**, 403–413 (2007).
44. K. Nishiizumi, Preparation of ^{26}Al AMS standards. *Nucl. Instrum. Methods Phys. Res. Sect. B* **223–224**, 388–392 (2004).
45. R. Braucher, S. Merchel, J. Borgomano, D. L. Bourlès, Production of cosmogenic radionuclides at great depth: A multi element approach. *Earth Planet. Sci. Lett.* **309**, 1–9 (2011).
46. J. O. Stone, Air pressure and cosmogenic isotope production. *J. Geophys. Res. Solid Earth* **105**, 23753–23759 (2000).
47. G. P. Compo, J. S. Whitaker, P. D. Sardeshmukh, N. Matsui, R. J. Allan, X. Yin, B. E. Gleason, R. S. Vose, G. Rutledge, P. Bessemoulin, S. Brönnimann, M. Brunet, R. I. Crouthamel, A. N. Grant, P. Y. Groisman, P. D. Jones, M. C. Kruk, A. C. Kruger, G. J. Marshall, M. Maugeri, H. Y. Mok, Ø. Nordli, T. F. Ross, R. M. Trigo, X. L. Wang, S. D. Woodruff, S. J. Worley, The twentieth century reanalysis project. *Q. J. Roy. Meteorol. Soc.* **137**, 1–28 (2011).
48. A. T. Codilean, Calculation of the cosmogenic nuclide production topographic shielding scaling factor for large areas using DEMs. *Earth Surf. Process. Landf.* **31**, 785–794 (2006).
49. K. Hippe, N. A. Lifton, Calculating isotope ratios and nuclide concentrations for in situ cosmogenic ^{14}C analyses. *Radiocarbon* **56**, 1167–1174 (2014).
50. D. Fink, M. Hotchkis, Q. Hua, G. Jacobsen, A. M. Smith, U. Zoppi, D. Child, C. Mifsud, H. van der Gaast, A. Williams, M. Williams, The ANTARES AMS facility at ANSTO. *Nucl. Instrum. Methods Phys. Res. Sect. B* **223–224**, 109–115 (2004).
51. A. M. Smith, Q. Hua, A. Williams, V. A. Levchenko, B. Yang, Developments in micro-sample ^{14}C AMS at the ANTARES AMS facility. *Nucl. Instrum. Methods Phys. Res. Sect. B* **268**, 919–923 (2010).
52. S. M. Fahrni, L. Wacker, H.-A. Synal, S. Szidat, Improving a gas ion source for ^{14}C AMS. *Nucl. Instrum. Methods Phys. Res. Sect. B* **294**, 320–327 (2013).

Acknowledgments: We acknowledge support from the University of Wollongong, GeoQuEST, and the Centre for Accelerator Science at ANSTO through the National Collaborative Research Infrastructure Strategy (NCRIS). We also wish to acknowledge the

Traditional Owners of this country. We thank F. J. Pazzaglia, R. McKeon, and one anonymous reviewer for suggestions on how to improve the clarity of the text. **Funding:** R.-H.F. acknowledges funding from the Australian Research Council (grant ARC LP170100155) and ANSTO (grant AP11418). **Author contributions:** R.-H.F. and A.T.C. conceived the study, wrote the paper, and performed field and laboratory work. K.M.W., A.M.S., D.F., B.Y., V.A.L., L.W., and T.F. performed AMS analyses of ^{10}Be, ^{26}Al, and ^{14}C and participated in data reduction. T.J.C. compiled the optically stimulated luminescence and thermoluminescence data, S.K.M. and N.S. performed fieldwork and contributed samples, and T.J.D. contributed to ^{14}C analyses. All authors discussed the results and commented on the manuscript. **Competing interests:** The authors declare that they have no competing interests. **Data and materials availability:** All data needed to evaluate the conclusions in the paper are present in the paper and/or the Supplementary Materials. Additional data related to this paper may be requested from the authors.

Submitted 16 October 2019
Accepted 8 May 2020
Published 19 June 2020
10.1126/sciadv.aaz8845

Citation: R.-H. Fülöp, A. T. Codilean, K. M. Wilcken, T. J. Cohen, D. Fink, A. M. Smith, B. Yang, V. A. Levchenko, L. Wacker, S. K. Marx, N. Stromsoe, T. Fujioka, T. J. Dunai, Million-year lag times in a post-orogenic sediment conveyor. *Sci. Adv.* **6**, eaaz8845 (2020).

Science Advances

Million-year lag times in a post-orogenic sediment conveyor

R.-H. Fülöp, A. T. Codilean, K. M. Wilcken, T. J. Cohen, D. Fink, A. M. Smith, B. Yang, V. A. Levchenko, L. Wacker, S. K. Marx, N. Stromsoe, T. Fujioka and T. J. Dunai

Sci Adv **6** (25), eaaz8845.
DOI: 10.1126/sciadv.aaz8845